MAPK13 controls structural remodeling and disease after epithelial injury

Kangyun Wu[1*], Yong Zhang[1*], Dailing Mao[1], Courtney A. Iberg[1], Huiqing Yin-Declue[1], Kelly Sun[1], Shamus P. Keeler[1], Hallie A. Wikfors[1], Deanna Young[1], Jennifer Yantis[1], Stephen R. Austin[1], Derek E, Byers[1], Steven L. Brody[1], Erika C. Crouch[2], Arthur G. Romero[1], and Michael J. Holtzman[1,3,4*]

[1]Pulmonary and Critical Care Medicine, Department of Medicine, [2]Department of Pathology and Immunology, and [3]Department of Cell Biology and Physiology, Washington University School of Medicine, St. Louis, MO 63110 and [4]NuPeak Therapeutics Inc., St. Louis, MO 63105

*Contributed equally.

Running title: MAPK13 control of remodeling

Address correspondence to Michael J. Holtzman., Washington University School of Medicine, Campus Box 8052, 660 South Euclid Avenue, St. Louis, MO 63110. Tel. 314-362-8970; E-mail: mjholtzman@wustl.edu.

Abbreviations used in this article: basal-ESC, basal-epithelial stem cell; CLCA1, chloride channel accessory 1; COPD, chronic obstructive pulmonary disease; Covid-19, coronavirus disease of 2019; hTEC, human tracheobronchial epithelial cell; MAPK, mitogen-activated protein kinase; MUC5AC, mucin 5AC; MUC5B, mucin 5B; SeV, Sendai virus.

Keywords: mitogen-activated protein kinase (MAPK), p38 kinase, epithelial stem cell, respiratory viral infection, asthma, chronic obstructive pulmonary disease (COPD).

Abstract

All living organisms are charged with repair after injury particularly at epithelial barrier sites, but in some cases this response leads instead to structural remodeling and long-term disease. Identifying the molecular and cellular control of this divergence is key to disease modification. In that regard, stress kinase control of epithelial stem cells is a rational entry point for study. Here we examine the potential for mitogen-activated protein kinase 13 (MAPK13) regulation of epithelial stem cells using models of respiratory viral injury and post-viral lung disease. We show that *Mapk13* gene-knockout mice handle acute infectious illness as expected but are protected against structural remodeling manifest as basal-epithelial stem cell (basal-ESC) hyperplasia-metaplasia, immune activation, and mucinous differentiation. In corresponding cell models, *Mapk13*-deficiency directly attenuates basal-ESC growth and organoid formation. Extension to human studies shows marked induction/activation of basal-cell MAPK13 in clinical samples of comparable remodeling found in asthma and COPD. Here again, *MAPK13* gene-knockdown inhibits human basal-ESC growth in culture. Together, the data identify MAPK13 as a control for structural remodeling and disease after epithelial injury and as a suitable target for down-regulation as a disease-modifying strategy.

New and noteworthy

This study identifies a distinct role for stress kinase MAPK13 in controlling the epithelial stem cell response to injury and the consequent development of tissue remodeling. The present model has direct implications for lung injury and subsequent disease triggered by respiratory viruses and other inhaled toxins, but the tissue distribution of MAPK13 implies related actions at other barrier sites. The findings also refine a hypothesis for therapeutic intervention based on proper scaling of MAPK13 function including down-regulation with selective kinase inhibitors.

Introduction

Organisms are constantly challenged with a wide spectrum of injuries and the need for a repair process to return to proper physiological function. While this goal is often achieved, in some cases, the process results in a skewed response that ends in structural remodeling and dysfunction of the injured tissue site. Therefore, it is key to define the cell and molecular controls of these outcomes to foster and preserve proper repair versus remodeling and abnormal function. This paradigm is particularly common at epithelial barrier sites wherein epithelial stem cells and stress-related signaling molecules orchestrate the response to injury from a host of environment agents. Notable among these molecules are an overlapping and interacting set of stress kinases presumably designed for redundancy and diversity. Thus, the complexity of this network has made it difficult to assign function to specific kinases and ultimately to modify kinase behavior that preserves or enhances repair to homeostatic conditions and prevents or reverses abnormal remodeling and disease. Thus, a first step remains to better identify stress kinase control of the epithelial repair and remodeling process after injury.

Among the candidates for study, the respiratory barrier in particular is exposed to inhaled toxins and infectious agents with every breath and therefore maintains an active sentinel system to restore integrity at the barrier site. Here again, however, the normal program for recovery can be skewed to an ongoing response that results in structural remodeling and disease. This divergence is especially manifest as long-term post-viral lung disease (PVLD) that can manifest as long-Covid, post-influenza sequelae and related virus-triggered diseases such as asthma and chronic obstructive pulmonary disease (COPD) (1-11). In that context, basal-epithelial stem cells (basal-ESCs) represent a stereotyped feature of the epithelial barrier program. In experimental models, this cell population can be reprogrammed for hyperplasia and metaplasia that disrupts lung function after native Sendai virus (SeV) or adapted influenza A virus (IAV) infections (3, 12-14). Similar activation of basal cell growth and differentiation is found in long-term Covid (4, 15).

Despite this understanding of cellular response, the molecular basis for epithelial stem cell growth and differentiation is less certain and is still vital to defining mechanism of repair and intervention to correct remodeling. One of the most studied kinase candidates is the mitogen activated protein kinase (MAPK) family of stress kinases, and among them, the original family member MAPK14 (aka p38α) is often proposed as a master regulator of the inflammatory response to damage (16). Unfortunately, this candidate strategy has not resulted in any measurable progress in modifying the response to lung injury or for that matter disease responses at any other tissue sites (17-19). As an alternative, our earlier studies of basal-ESCs cultured from human airways identified a related but distinct CMGC family member known as MAPK13 (aka MAPK-p38δ) (1) that emerged as a more dominant control of basal-ESC differentiation to mucous cells (1). This finding was intriguing given the primordial nature of mucinous differentiation in

host defense and the invariant appearance of a mucinous phenotype in PVLD and related virus-triggered diseases such as asthma, COPD, and long-term Covid (1, 3, 4, 7, 20-22). The fundamental nature of this control mechanism also derives from studies that implicate MAPK13 in diseases that include diabetes, sepsis, and cancer (23-28). Given this unexplained diversity, we questioned here whether MAPK13 might represent a fundamental control for epithelial stem cell reprogramming with structural remodeling and disease endpoints. The downstream capability for MAPK13 interaction with multiple kinase substrates in epithelial and perhaps sentinel immune cells would thereby explain the broad range of disease phenotypes. The present study therefore addresses whether MAPK13 might be essential for basal-ESC reprogramming using a relatively simple but well-controlled gene knockout or knockdown approach based also in a well-characterized model of the epithelial and immune cell response to viral injury (1-3, 14, 29-39). Together, the experimental approaches provide a paradigm for epithelial barrier cells in balancing tissue repair versus structural remodeling and disease and a method to restore this balance as a disease-modifying strategy.

Results

Mapk13 gene knockout prevents PVLD in a mouse model

As introduced above, MAPK13 function was implicated in mucinous differentiation in human airway epithelial cells in culture (1). However, any corresponding role for MAPK13 alone in regulating mucus production in vivo or other aspects of basal epithelial cell reprogramming (particularly cell growth or immune activation) in any model still needed to be better defined. To address these issues, we engaged a mouse model that resembles lung diseases (asthma, COPD, and Covid-19) that are linked to respiratory viral infection in humans (1-4). In this model, infection with a natural pathogen Sendai virus (SeV) manifests a stereotyped (top-down) pattern of infection followed by PVLD and thereby maintains fidelity to the pattern of acute and chronic disease found in humans (1-3, 14, 29-39). To assess target function, we generated *Mapk13*$^{-/-}$ mice (**Supplemental Figure 1A,B**) that manifested similar acute infectious illness to wild-type (WT) mice as tracked by weight loss and lung levels of viral RNA (**Figure 1A,B**). Despite clearance of infectious virus, lung levels of Mapk13 continued to increase during the development of chronic lung disease based on immunoblotting (**Figure 1C**) and localized to Krt5^{+} basal epithelial cells in remodeling regions based on immunostaining (**Figure 1D,E**). This staining was not detected in *Mapk13*$^{-/-}$ mice as a sign of antibody specificity **(Figure 1D,E).** Further, Mapk13 was primarily nuclear consistent with phosphorylation/activation and control of basal cell growth since both signals were decreased in *Mapk13*$^{-/-}$ mice. Relatedly, basal cell hyperplasia (marked by Aqp3^{+} basal-epithelial cell levels) were decreased in vivo (**Figure 1F-H**). Further, reprogramming for basal-ESC growth (marked by organoid-forming capacity) or immune activation (marked by *Cxcl17* mRNA induction with GPNMB stimulation) (42) were both decreased in 3D cultures from *Mapk13*$^{-/-}$ compared to WT control mice (**Figure 1I**). In

contrast, myeloid cell growth was no different under *Mapk13*$^{-/-}$ conditions based on comparable conditions for bone-marrow derived dendritic cell (BMDC) or monocyte-macrophage (BMM) cultures (**Figure 1J**).

Consistent with these findings, lung immunostaining showed that the epithelial-cell proliferation pool (marked by Ki-67) and corresponding basal-cell expansion (marked by Krt5) were markedly attenuated in *Mapk13*$^{-/-}$ mice (**Figure 2A,B**). Together, these phenotypes translated to attenuation of periodic acid Schiff (PAS) and hematoxylin tissue staining (reflecting mucus production and cellularity, respectively) in lung sections at 49 d after SeV infection when structural remodeling and PVLD is otherwise maximal (**Figure 2C**). Each of the improvements in structural remodeling and histopathology in *Mapk13*$^{-/-}$mice was significant compared to WT control mice based on quantitative morphology (**Fig. 2D**). The same pattern of remodeling and histopathology was also found at 21 d after SeV infection (**Supplemental Fig. 2A-D**), when disease phenotype is initially significant. This data provides for a precise and progressive pathway for PVLD in the present mouse model.

In concert with attenuation of remodeling and histopathology, *Mapk13*$^{-/-}$ mice also showed significant down-regulation of specific biomarkers designed to track disease based on lung tissue mRNA levels. Significant biomarker decreases included: basal-ESC growth marked by *Krt5, Aqp3*, and *Trp63*; immune activation marked by *Serpinb2*, *Ltf, Cxcl17,* and *Nos2*; type 2 inflammation marked by *Il13, Arg1,* and *Trem2,* type 1/2 inflammation marked by *Il6*; and mucinous differentiation marked by *Muc5ac* and *Clca1* (**Figure 3A-E**). The *Muc5b* mRNA signal for mucinous differentiation was relatively weak (**Figure 3E**), but this finding might be due to post-transcriptional regulation of Muc5b expression. As expected, *Mapk13* gene induction/expression was lost in *Mapk13*$^{-/-}$ mice (**Figure 3F**). No *Mapk13*-dependent attenuation was found for the alarmin signal marked by *Il33* mRNA (**Figure 3G**), consistent with IL-33 expression predominantly in alveolar epithelial type 2 (AT2) cells versus basal cells in mouse lungs (3, 14, 37). We also detected no significant induction and hence no consequent blockade of conventional type 1 inflammation marked by *Ifng, Tnfa,* and *Il1b* mRNA levels (**Figure 3H**), consistent with the that data that this signal (that is often MAPK14-dependent) is not a primary driver for PVLD (1, 45, 46). The same pattern of biomarker induction and blockade was also found at 21 d after SeV infection (**Supplemental Figure 3A-H**), a time point when PVLD is nearly fully developed. This data again supports the role of a precisely defined pathway to long-term disease after viral injury in this model.

In line with the effects on mRNA biomarkers, we also found correction of clinical disease phenotypes: immune activation based on Nos2^{+} immunostaining (**Figure 4A,B**); macrophage infiltration based on F4/80^{+} immunostaining (**Figure 4C,D**); and mucinous differentiation based on immunostaining for Muc5ac and Muc5b (**Figure 4E,F**). This pattern of disease phenotypes is consistent with biomarkers of airway disease in humans (1, 3, 4, 7, 21, 44). To further define whether the downregulation of these disease

biomarkers translated to improvements in pulmonary function, we also checked levels of oxygenation and airway reactivity that are also regularly associated with post-viral and related airway disease conditions. Notably, these readouts showed improvements in hypoxemia monitored by SpO_2 using oximetry (**Figure 5A**) and attenuation of airway hyperreactivity assessed using inhaled methacholine challenge (**Figure 5B**). Together, these findings provide support for a therapeutic effect of targeting Mapk13 as a strategy to improve pulmonary function in PVLD and related conditions.

MAPK13 **gene knockdown attenuates basal-ESC growth in a human model**

To extend our experimental findings from mouse models to humans, we first assessed whether MAPK13 expression and activation might be found in lung diseases linked to similar basal-ESC reprogramming and structural remodeling after respiratory viral infections or other inhaled agents of injury and inflammation. Towards that aim, we studied lung tissue samples from disease conditions that implicated basal-ESC reprogramming for excess growth, immune activation, and mucinous differentiation (1-4). Given the challenge of obtaining lung tissue samples in the setting of severe viral infections, we reasoned that a renewable stem cell population might maintain a long-term program for structural remodeling. In that context, we characterized lung tissue samples from chronic asthma and COPD patients that were obtained as described previously (1, 3). With that approach, immunostaining of lung sections showed markedly increased expression of MAPK13 in these disease conditions compared to non-disease controls (**Figure 6A**). Further, and similar to IL-33 expression in mice and humans, we found MAPK13 expression was often localized to $KRT5^+$ basal epithelial cells that were found in airway epithelium in asthma and COPD (**Figure 6A**). In addition, MAPK13 expression was often further localized to a nuclear site, consistent with phosphorylation/activation and nuclear translocation that is typical of MAPK and kinase signaling in general (47). The findings fit with MAPK13 function in type 2 immune signaling for mucinous differentiation in human airway epithelial cells in culture (1). However, any corresponding role for MAPK13 in regulating other aspects of basal epithelial cell reprogramming (particularly cell growth) in humans still needed to be defined.

To address this issue, we extended our analysis of human samples to hTEC culture models where growth can be monitored independent of immune cell signals. To assess basal-ESC growth, hTECs were maintained under submerged culture conditions that preserve basal-ESC growth and inhibit differentiation to basal-lineage cells in the absence of an air-liquid interface (3). We also established parameters for specific *MAPK13* gene knockdown using a newly applied method for anti-sense oligonucleotide (ASO) to target *MAPK13* mRNA. This approach demonstrated specific decreases in MAPK13 protein (**Figure 6B,C**) and corresponding downregulation of basal-ESC growth under these conditions (**Figure 6D,E**). Together,

these results provide evidence that MAPK13 is overexpressed, activated, and susceptible to therapeutic blockade in human basal-ESCs s as predicted by our mouse model.

Discussion

In this study, we use gene-knockout strategies to identify MAPK13 as a critical control point for structural remodeling and consequent disease after epithelial injury. Key findings include: (1) *Mapk13* gene knockout alone is sufficient to attenuate basal-ESC reprogramming for hyperplasia/metaplasia, immune activation, and mucinous differentiation in a mouse model of epithelial injury due to respiratory viral infection; and (2) *MAPK13* gene knockdown in a corresponding human basal-ESC culture model similarly down-regulates basal-ESC growth in culture. Both mouse and human studies localize MAPK13 induction and activation to basal epithelial cells in situ during remodeling and disease. The data thereby define MAPK13 as a practical target for modifying the tissue remodeling and dysfunction that can develop after epithelial injury in the lung and likely other barrier sites as diagrammed in **Figure 7**. Here we highlight three aspects of this research progress.

First, an important premise of the present study was that the definition of MAPK13 function remained incomplete despite previous studies of MAPK13 deficiency in gene-knockout mice. Some of the uncertainty was due to the frequent performance of MAPK13 studies in combination with MAPK12 deficiency, based on the similar protein sequence/structure and in some cases tissue distribution of these two potentially redundant kinases (27, 48-54). Given the present results, it is rational to consider the function of MAPK13 on its own. In that regard, MAPK13 solo function has been detected in mouse models of neutrophil infiltration in LPS-induced lung injury (25), pancreatic beta-cell secretion of insulin (24), LPS-induced lung injury (25), and keratinocyte hyperplasia after carcinogenic stimulation (26). However, these previous studies did not precisely localize MAPK13 expression and activation as done the present analysis using tissue immunostaining and corresponding cell isolation. Thus, the site of action for MAPK13 was generally inferred from related ex vivo experiments. Despite this drawback, the overlap of the present findings with basal cell hyperplasia after epithelial injury in the lung appear to overlap with a similar phenotype in skin and the related theme of epithelial stem cell growth. This connection further reinforces the proposal for a role for MAPK13 in epithelial barrier repair and remodeling after injury. It is also possible that this repair process requires MAPK13 coordination of cell growth with cell migration, immune activation, differentiation, and secretion based on downstream connection to diverse kinase substrates and in turn disease phenotypes.

Second, and relevant to this apparent spectrum of stress kinase function, the present findings also come in the context of our previous work on MAPK13 in human cell and mouse models of chronic lung disease and corresponding analysis of lung tissue samples from this type of disease. These earlier studies first uncovered

a role for MAPK13 in controlling basal-ESC differentiation to mucous cells in concert with MAPK13 induction/activation in chronic respiratory disease (1). In this initial work, definition of function relied on study of human basal-ESC cultures subject to siRNA-mediated gene-knockdown or treatment with a relatively weak MAPK13 inhibitor (NuP-43; BIRB-796) and first-generation compounds that improved MAPK13 enzyme inhibition but maintained broad kinase activity (1). Subsequently, this approach was extended to a second-generation MAPK13-14 inhibitor (designated NuP-3) that was also effective in blocking mucus production in hTEC cell cultures and prevented airway inflammation and mucus production in minipig models of disease using cytokine-challenge and viral-infection (45). However, these models manifested only short-term inflammation and mucus production without the full features of long-term basal-ESC hyperplasia/metaplasia found in the presently used mouse model and in humans (3, 4, 14, 34, 35). The present work advances these previous approaches by showing that MAPK13 alone can also control basal-ESC growth based on more specific techniques for gene-knockout in vivo in mice and in vitro in human basal cell culture. The findings thereby suggest a more fundamental role for MAPK13 in the response to epithelial barrier injury and an opportunity to improve barrier function based on the present lung physiology readouts for blood/tissue oxygenation and airway reactivity.

With this advance, we expect the present data to provide an alternative to the conventional focus on related stress kinases in inflammatory disease, including lung disease. More specifically, there has been primary attention to the related kinase MAPK14 as a functional and therapeutic target of interest (17, 55-65). Indeed, in models of inflammatory disease, MAPK14-specific inhibitors are highly effective in blocking cytokine (e.g., TNF-α and IL-1β) production and/or signal transduction (66). This mechanism predicted therapeutic benefit in a variety of conditions including acute and chronic respiratory diseases (67). However, even the most advanced versions of these candidate drugs have not proved effective in clinical trials of patients with chronic lung disease due to COPD where these types of cytokines are found at higher levels (59). The data here suggest a basis for this failure by implicating the independent action of MAPK13 in a disease process that is instead linked to type 2 inflammation. This connection is illustrated by the present biomarker panel that features this alternative type of inflammation (marked especially by cytokine IL-13 expression). In contrast, the biomarkers for conventional inflammation (TNF-α and IL-1β) showed no significant induction in the present model of structural remodeling and chronic lung disease that developed after viral injury.

Third, despite the MAPK13 link to epithelial cells, the present data does not exclude an additional role for MAPK13 function in immune cells, particularly those participating in the type 2 immune response as a stereotyped feature of tissue repair and remodeling. In that regard, we provided evidence of monocyte-derived dendritic cell (moDC) action upstream along with macrophage, innate lymphoid cell type 2 (ILC2), and NKT cell action downstream of basal-ESC activation (2, 33, 36, 37). These epithelial-immune cell

collaborations thereby provide a feed-forward mechanism for the observed combination of disease phenotypes (basal-ESC hyperplasia/metaplasia, type 2 inflammation, and excess mucus production). These phenotypes are characteristic of PVLD in mice and related lung diseases in humans as validation of the present biomarker panel. Defining the precise role of each epithelial-stem cell and immune-cell population is a challenging goal of future studies. Thus, conditional knockout strategies for basal-ESCs can change baseline conditions (14, 68) when targeting genes such as MAPK13 and related members of the CMGC kinase superfamily that regulate cell cycle (28, 69). Further, selective down-regulation of specific myeloid cell subsets is still imprecise with existing tools. Nonetheless, these cell-specific strategies are ongoing in experiments using human cell culture and animal models to provide better definition of MAPK13 function.

In sum, the present data solidify the proposal for a primordial response to epithelial injury that depends on MAPK13 and suggest a MAPK13-targeted strategy to improve this response if it skews to structural remodeling and disease. The results also highlight one of the most common forms of epithelial injury in the form of respiratory viral infection. Significant evidence exists that this same pattern of epithelial and immune cell responses develops after injury due to a broad spectrum of respiratory viruses (including human enterovirus, influenza virus, respiratory syncytial virus, and human rhinovirus) and other inhaled agents (such as airborne pollutants) (34, 35, 70-72). In each case, there is experimental and clinical evidence for initiation, progression, and/or exacerbation of chronic respiratory diseases. The tissue distribution of MAPK13 suggests that it might provide a similar function at other sites and forms of tissue injury. Future studies should provide a coherent picture of epithelial injury, remodeling, and corresponding therapy using the present findings as a more specific guideline for a correctable target kinase.

Materials and Methods

Mouse models

Male and female wild-type (WT) C57BL/6J mice (000664) mice were obtained from Jackson Laboratory. The *Mapk13* gene knockout mice (*Mapk13*$^{-/-}$) were generated in the C57BL/6J background using CRISPR/Cas9 technology with gRNAs that were designed to target early in exon 1 based on a sequence to minimize any off-target effect. Synthetic gRNAs were purchased from IDT Technologies and complexed with recombinant Cas9 protein before nucleofection in Neuro 2a cells for validation. The selected gRNA (tacctgccgcccgcgcacg) cleaved 8 nucleotides (cgtcggca) that resulted in a reading frame shift and stop codon introduction in exon 2 of the *Mapk13* gene. The ribonucleoprotein complex containing Cas9 protein (1 μg/μl) and gRNA (0.3 μg/μl) was then electroporated into single-cell embryos of C57BL/6J mice, and 25–30 eggs were transferred into each pseudo-pregnant female to generate founder mice. Knockout founders were identified by analyzing the PCR-amplified target region (forward primer 5′-ggaacgtacctgggcgag and reverse primer 5′-gtcccacgaactccgagatc) using next-generation sequencing to identify out-of-frame indels. Heterozygous F1 mice were obtained from matings between founders and WT mice, and homozygous F2 mice were obtained through sibling matings of F1 mice. The resulting *Mapk13*$^{-/-}$ mice were found to reproduce

and develop normally relative to WT control mice.

All mice were maintained and co-housed in a barrier facility using cages fitted with micro-isolator lids. Animal husbandry and experimental procedures were approved by the Animal Studies Committees of Washington University School of Medicine in accordance with the guidelines from the National Institutes of Health. Sendai virus (SeV, Sendai/52 Fushimi strain, ATCC VR-105) was obtained from ATCC and prepared and titered by plaque-forming assay and qPCR assay as described previously (2). Mice were infected with SeV (2.6 x 10^5 PFU) as described previously (35). Virus or an equivalent amount of UV-inactivated virus or PBS alone was delivered intranasally in 30 µl of PBS under ketamine/xylazine anesthesia at 6-9 wk of age. Results from male and female mice were pooled since no significant differences were found between sexes as reported initially (40) and confirmed recently (35) and in the present experiments (data not shown). Viral titers for stock solutions and lung infections were monitored by quantitative PCR (qPCR) assay using primers for SeV-*NP* RNA as defined previously and in **Supplemental Table 1** using *SeV-NP*-expressing plasmids as an internal standard (35)

Immunoblotting

For western blotting, lung tissue or cultured cells were lysed in RIPA buffer (ThermoFisher) supplemented with PhosSTOP (Sigma) and cOmplete PIC (Sigma) for 30 min at 4 ºC. Tissue was homogenized in bead tubes and cell lysates were sheared 7 times with a 29G needle, and all samples were centrifuged at 14,100 x g at 4 ºC. The supernatant was aliquoted and stored at -80ºC until needed. Protein concentration was determined with the bicinchoninic acid (BCA) protein assay kit (ThermoFisher). Lysate (40-50 µg) was loaded into 4-15% Mini-PROTEAN® TGX gels (Bio-Rad) and separated by SDS-PAGE electrophoresis. Proteins were transferred to nitrocellulose membranes using a Trans-Blot® Turbo blot transfer pack (Bio-Rad). Nitrocellulose membranes were blocked with Odyssey blocking buffer (Li-COR Biosciences) and then primary antibodies for MAPK13 (AF1519, R&D), β-actin (ab8224, Abcam), or Gapdh (MAB374, Sigma) were incubated overnight at 4 ºC in Odyssey blocking buffer with 0.2% Tween-20. Membranes were washed with 0.1% PBS-Tween-20 and then incubated with anti-mouse or anti-rabbit secondary antibodies (Li-COR) in Odyssey blocking buffer with 0.2% Tween-20 for 1 at 25 °C. Membranes were washed with 0.1% PBS-Tween-20, and protein bands were detected using an Odyssey CLx infrared imaging system (LI-COR Biosciences).

Flow cytometry and FACS

Single cell suspensions were generated from minced lung tissue that was subjected to collagenase (Liberase TM Research Grade, Roche), hyaluronidase (Sigma), DNAse I (Sigma), and Dispase II (Roche) digestion for 45 min at 37 °C and then treated with ACK buffer (Lonza) to remove red blood cells. Following FcR blockade, lung cell suspensions were incubated with labeled antibodies and were sorted using a Sony SY3200 Synergy high-speed cell sorter. The following antibodies were used: anti-mouse CD31 (clone MEC 13.3; BD Biosciences), anti-mouse CD45 (clone 30-F11; BD Biosciences), anti-mouse EpCAM (clone G8.8; BioLegend), anti-Aqp3 (Abcam) and anti-Ki-67 (clone SolA15, eBiosciences). Anti-Aqp3 antibody was labeled using the Zenon antibody labeling kit (Molecular Probes). FACS results were plotted and analyzed using FlowJo software (TreeStar).

Tissue histology and staining

Lung tissue was fixed with 10% formalin, embedded in paraffin, cut into 5-µm sections and adhered to charged slides. Sections were stained with PAS and hematoxylin as described previously (14, 35). For immunostaining, sections were deparaffinized in Fisherbrand® CitriSolv® (Fisher), hydrated, and heat-treated with antigen unmasking solution (Vector Laboratories, Inc). Immunostaining was performed with the commercially available primary antibodies detailed in **Supplemental Table 2** and a rabbit anti-CLCA1 antibody described previously (1). Primary Abs were detected with secondary Abs labeled with Alexa Fluor 488 (Thermo Fisher Scientific) or Alexa Fluor 594 (Thermo Fisher Scientific) followed by DAPI counterstaining. Slides were imaged by light microscopy using a Leica DM5000 B and by immunofluorescent microscopy using an Olympus BX51, and staining was quantified in whole lung sections using a NanoZoomer S60 slide scanner (Hamamatsu) and ImageJ software as described previously (14, 35).

RNA analysis

RNA was purified from homogenized lung tissue using Trizol (Invitrogen) or from isolated cells with the RNeasy mini kit (Qiagen) and was used to generate cDNA with the High-Capacity cDNA Archive kit (Life Technologies). We quantified target mRNA and viral RNA levels using real-time qPCR assay with specific fluorogenic probe-primer combinations and Fast Universal PCR Master Mix systems (Applied Biosystems) with mouse-specific forward and reverse primers and probes as described previously (36) and in **Supplemental Table 3**. For the *Mapk13* assay, primers and probe were designed to amplify WT but not *Mapk13* indel sequence in *Mapk13*$^{-/-}$ mice. All samples were assayed using the 7300HT or QuantStudio 6 Fast Real-Time PCR System and analyzed using Fast System Software (Applied Biosystems). All real-time PCR data was normalized to the level of *Gapdh* mRNA. Values were expressed as fold-change based on the delta-delta Ct method as described previously (41).

Lung function tests

To test lung function, we assessed blood oxygen saturation (SpO_2) and airway reactivity to methacholine (MCh) as described previously (14). For SpO_2 monitoring, we used a MouseSTAT® pulse oximeter (Kent Scientific, Torrington, CT) applied to the paw skin under isoflurane anesthesia as described previously (14). To decrease variability in readings for this procedure, anesthetized mice were placed on the RightTemp warming pad, and the SpO_2 reading was recorded when the Oxiwave signal was stable. For airway reactivity measurements, the response to inhaled methacholine was determined by monitoring respiratory system resistance (R_{RS}) as described previously (14).

Mouse and human epithelial cell culture

For mouse epithelial cell cultures, lung epithelial cells from FACS (as described above) were resuspended in SAGM (Lonza) mixed 1:1 with growth-factor reduced Matrigel (BD Biosciences) and plated at 3 x 10^3 cells per 100 µL in 24-well Transwells (Corning). For the first 5 d, SAGM was added with 10 µM Rock inhibitor (Sigma) but without FBS. After 5 d, SAGM was added with 10 % FBS but without Rock inhibitor. The medium was changed every 2-3 d. Organoids were cultured with media alone for 14 d to monitor stem cell growth (using organoid levels) and with media plus GPNMB to monitor immune activation (using *Cxcl17* mRNA) as described previously (42). For human epithelial cell cultures, human tracheal and bronchial epithelial cells (hTECs) were isolated by enzymatic digestion and cultured

under submerged conditions as described previously (3). For the present experiments, hTECs were cultured in 96-well plate (2 x 10^4 cells per well) with two distinct AUMsilence FANA oligonucleotides specific for *Mapk13* mRNA and a scrambled control (AUM BioTech), with each ASO added to cells at 1 μM final concentration on culture days 1 and 3. Cell growth was assessed on culture day 5 using the CyQUANT cell viability assay (ThermoFischer) along with MAPK13 protein level using western blot as described above.

Human clinical samples

For asthma, COPD, and non-disease control samples, lung tissue was obtained from our Advanced Lung Disease Tissue Registry that contains whole lung explants harvested from consented patients in our lung transplant program; lungs that were not usable for transplantation from the local Organ Procurement Organization, Mid-America Transplant; and lungs from a tissue procurement service (IIAM, Edison, NJ) as described previously (1, 4, 43, 44). Human studies were conducted with protocols approved by the Washington University (St. Louis, MO) Institutional Review Board and USAMRDC Office of Research Protections. Clinical characteristics of tissue donors are provided in **Supplemental Table 4**.

Statistical analysis

All data are presented as mean and s.e.m. and are representative of at least three experiments with at least 5 data points per experiment. For cell and molecular data, unpaired student's t-test with Bonferroni correction as well as mixed-model repeated measures analysis of variance with Tukey correction for multiple comparisons were used to assess statistical significance between means. In all cases, significance threshold was set at $P < 0.05$. For physiological data, airway reactivity was assessed using either two-way repeated measures analysis of variance or restricted maximum likelihood linear mixed model with genotype, infection, and methacholine dose as fixed effects and subject as a random effect.

Acknowledgments

We thank the Pulmonary Morphology Core, Pathology-Immunology Transgenic-Microinjection Core, Genome Technology Access Core, Genome Engineering and iPSC Center, Anatomic and Molecular Pathology Core Labs, and Division of Comparative Medicine for technical support.

Funding

This work was supported by grants from the National Institutes of Health (National Heart, Lung, and Blood Institute UH2-HL123429, R35-HL145242, and STTR R41-HL149523, National Institute of Allergy and Infectious Diseases R01 AI130591, Department of Defense TTDA W81XWH2010603 and W81XWH2210281, Harrington Discovery Institute, and Hardy Trust Fund.

Disclosures

MJH is the Founder of NuPeak Therapeutics, Inc. KW, YZ, AGR, and MJH are inventors on a patent for MAPK inhibitors and methods of use thereof.

Author contributions

K.W. performed mouse, cell, and human tissue experiments; Y.Z. generated *Mapk13*$^{-/-}$ mice and performed mouse and cell experiments; D.M. performed mouse and cell experiments; C.A.I performed mouse and cell experiments; H.Y-D. performed immunostaining experiments; K.S. performed mouse experiments; S.P.K. performed mouse and cell experiments; H.A.W. performed cell experiments; D.Y. performed mouse experiments; J.Y. performed cell experiments, S.R.A. obtained and registered human samples; D.E.B. obtained and registered human samples, S.L.B. generated human epithelial cell samples, .E.C.C. analyzed histology; A.G.R. analyzed kinase-related data;, and M. J. H. directed the project and wrote the manuscript.

References

1. Alevy Y, Patel AC, Romero AG, Patel DA, Tucker J, Roswit WT, Miller CA, Heier RF, Byers DE, Brett TJ, and Holtzman MJ. IL-13–induced airway mucus production is attenuated by MAPK13 inhibition. *J Clin Invest.* 2012;122:4555-68.

2. Kim EY, Battaile JT, Patel AC, You Y, Agapov E, Grayson MH, Benoit LA, Byers DE, Alevy Y, Tucker J, Swanson S, Tidwell R, Tyner JW, Morton JD, Castro M, Polineni D, Patterson GA, Schwendener RA, Allard JD, Peltz G, and Holtzman MJ. Persistent activation of an innate immune response translates respiratory viral infection into chronic lung disease. *Nat Med.* 2008;14:633-40.

3. Byers DE, Alexander-Brett J, Patel AC, Agapov E, Dang-Vu G, Jin X, Wu K, You Y, Alevy YG, Girard J-P, Stappenbeck TS, Patterson GA, Pierce RA, Brody SL, and Holtzman MJ. Long-term IL-33-producing epithelial progenitor cells in chronic obstructive lung disease. *J Clin Invest.* 2013;123:3967-82.

4. Wu K, Zhang Y, Yin Declue H, Austin SR, Byers DE, Crouch EC, and Holtzman MJ. Lung remodeling regions in long-term coronavirus disease 2019 feature basal epithelial cell reprogramming. *Am J Pathol* 2023;193:680-9.

5. Dunican EM, Elicker BM, Gierada DS, Nagle SK, Schiebler ML, Newell JD, Raymond WW, Lachowicz-Scroggins ME, Di Maio S, Hoffman EA, Castro M, Fain SB, Jarjour NN, Israel E, Levy BD, Erzurum SC, Wenzel SE, Meyers DA, Bleecker ER, Phillips BR, Mauger DT, Gordon ED, Woodruff PG, Peters MC, and Fahy JV. Mucus plugs in patients with asthma linked to eosinophilia and airflow obstruction. *J Clin Invest.* 2018;128:997-1009.

6. Toda M, Tulic MK, Levitt RC, and Hamid Q. A calcium-activated chloride channel (HCLCA1) is strongly related to IL-9 expression and mucus production in bronchial epithelium of patients with asthma. *J Allergy Clin Immunol.* 2002;109(2):246-50.

7. Tang M, Elicker BM, Henry T, Gierada DS, Schiebler ML, Huang BK, Peters MC, Castro M, Hoffman EA, Fain SB, Ash SY, Choi JY, Hall C, Phillips BR, Mauger DT, Denlinger LC, Jarjour NN, Israel E, Phipatanakul W, Levy BD, Wenzel SE, Bleecker ER, Woodruff PG, Fahy JV, Dunican EM, and Program-3 NSAR. Mucus plugs persist in asthma, and changes in mucus plugs associate with changes in airflow over time. *Am J Respir Crit Care Med.* 2022;205:1036-45.

8. Hogg JC, Chu F, Utokaparch S, Woods R, Elliott WM, Buzatu L, Cherniack RM, Rogers RM, Sciurba FC, Coxson HO, and Pare PD. The nature of small-airway obstruction in chronic obstructive pulmonary disease. *N Eng J Med.* 2004;350:2645-53.

9. Ekberg-Aronsson M, Pehrsson K, Nilsson JA, Nilsson PM, and Lofdahl CG. Mortality in GOLD stages of COPD and its dependence on symptoms of chronic bronchitis. *Respir Res.* 2005;6:98.

10. Hogg JC, Chu FS, Tan WC, Sin DD, Patel SA, Pare PD, Martinez FJ, Rogers RM, Make BJ, Criner GJ, Cherniack RM, Sharafkhaneh A, Luketich JD, Coxson HO, Elliott WM, and Sciurba FC. Survival after lung volume reduction in chronic obstructive pulmonary disease: insights from small airway pathology. *Am J Respir Crit Care Med.* 2007;176(5):454-9.

11. Kesimer M, Ford AA, Ceppe A, Radicioni G, Cao R, Davis CW, Doerschuk CM, Alexis NE, Anderson WH, Henderson AG, Barr RG, Bleecker ER, Christenson SA, Cooper CB, Han MK, Hansel NN, Hastie AT, Hoffman EA, Kanner RE, Martinez F, Paine Rr, Woodruff PG, O'Neal WK, and Boucher RC. Airway mucin concentration as a marker of chronic bronchitis. *N Engl J Med.* 2017;377:911-22.

12. Zuo W, Zhang T, Zheng D, Wu A, Guan SP, Liew A-A, Yamamoto Y, Wang X, Lim SJ, Vincent M, Lessard M, P. CC, Xian W, and McKeon F. p63+Krt5+ distal airway stem cells are essential for lung regeneration. *Nature.* 2015;517:616-20.

13. Vaughan AE, Brumwell AN, Xi Y, Gotts JE, Brownfield DG, Treutlein B, Tan K, Tan V, Liu FC, Looney MR, Matthay MA, Rock JR, and Chapman HA. Lineage-negative progenitors mobilize to regenerate lung epithelium after major injury. *Nature.* 2015;517:621-5.

14. Wu K, Kamimoto K, Zhang Y, Yang K, Keeler SP, Gerovac BJ, Agapov EV, Austin SP, Yantis J, Gissy KA, Byers DE, Alexander-Brett J, Hoffmann CM, Wallace M, Hughes ME, Morris SA, and Holtzman MJ. Basal-epithelial stem cells cross an alarmin checkpoint for post-viral lung disease. *J Clin Invest.* 2021;131:e149336.

15. Delorey TM, Ziegler CGK, Heimberg G, Normand R, Yang Y, Segerstolpe A, Abbonddanza D, Fleming SJ, Subramanian A, Montoro DT, Jagadeesh KA, Dey KD, Sen P, Slyper M, Pita-Juarez YH, and Phillips D. COVID-19 tissue atlases reveal SARS-CoV-2 pathology and cellular targets. *Nature.* 2021;595:107-13.

16. Han J, Wu J, and Silke J. An overview of mammalian p38 mitogen-activated protein kinases, central regulators of cell stress and receptor signaling. *F1000Res.* 2020;9.

17. Haller V, Nahidino P, Forster M, and Laufer SA. An updated patent review of p38 MAPK kinase inhibitors (2014-2019). *Expert Opin Ther Pat.* 2020;30:453-66.

18. Pelaia C, Vatre, A., Gallelli L, Lombardo N, Sciacqua A, Savino R, and Pelaia G. Role of p38 mitogen-activated protein kinase in asthma and COPD: pathogenic aspects and potential targeted therapies. *Drug Design, Development and Therapy.* 2021;15:1275-84.

19. Martucci C, Allen AD, Moretto N, Bagnacani V, Fioni A, Patacchini R, Civelli M, Villetti G, and Facchinetti F. CHF6297: a novel potent and selective p38 MAPK inhibitor with robust anti-inflammatory activity and suitable for inhaled pulmonary administration as dry powder. *Front Pharmacol.* 2024;15:1343941.

20. Aikawa T, Shimura S, Sasaki H, Ebina M, and Takishima T. Marked goblet cell hyperplasia with mucus accumulation in the airways of patients who died of severe acute asthma attack. *Chest.* 1992;101:916-21.

21. Radicioni G, Ceppe A, Ford AA, Alexis NE, Barr RG, Bleecker ER, Christenson SA, Cooper CB, Han MK, Hansel NN, Hastie AT, Hoffman EA, Kanner RE, Martinez FJ, Ozkan E, Paine R, 3rd, Woodruff PG, O'Neal WK, Boucher RC, and Kesimer M. Airway mucin MUC5AC and MUC5B concentrations and the initiation and progression of chronic obstructive pulmonary disease: an analysis of the SPIROMICS cohort. *Lancet Respir Med.* 2021;9(11):1241-54.

22. Kato T, Asakura T, Edwards CE, Dang H, Mikami Y, Okuda K, Chen G, Sun L, Gilmore RC, Hawkins P, De la Cruz G, Cooley MR, Bailey AB, Hewitt SM, Chertow DS, NIH COVID-19 Autopsy Consortium, Borczuk AC, Salvatore S, Martinez FJ, Thorne LB, Askin FB, Ehre C, Randell SH, O'Neal WK, Baric RS, and Boucher RC. Prevalence and mechanisms of mucus accumulation in COVID-19 lung disease. *Am J Respir Crit Care Med.* 2022;206:1336-52.

23. Goedert M, Hasegawa M, Jakes R, Lawler S, Cuenda A, and Cohen P. Phosphorylation of microtube-associated protein tau by stress-activated protein kinases. *FEBS Lett.* 1997;409:57-62.

24. Sumara G, Formentini I, Collins S, Sumara I, Windak R, Bodenmiller B, Ramracheya R, Caille D, Jiang H, Platt KA, Meda P, Aebersold R, Rorsman P, and Ricci R. Regulation of PKD by the MAPK p38δ in insulin secretion and glucose homeostasis. *Cell.* 2009;136:235-48.

25. Ittner A, Block H, Reichel CA, Varjosalo M, Gehart H, Sumara G, Gstaiger M, Krombach F, Zarbock A, and Ricci R. Regulation of PTEN activity by p38d-PKD1 signaling in neutrophils confers inflammatory responses in the lung. *J Exp Med.* 2012;209:2229-46.

26. Schindler E, Hindes A, Gribben E, Burns C, Yin Y, Lin M, Owen R, Longmore G, Kissling G, Arthur J, and Efimova T. p38delta Mitogen-activated protein kinase is essential for skin tumor development in mice. *Cancer Res.* 2009;69:4648-55.

27. Risco A, Del Fresno C, Mambol A, Alsina-Beauchamp D, MacKenzie KF, Yang H-T, Barber DF, Morcelle C, Arthur JSC, Ley SC, Ardavin C, and Cuenda A. p38g and p38d kinases regulate the Toll-like receptor 4 (TLR4)-induced cytokine production by controlling ERK1/2 protein kinase pathway activation. *American Review of Respiratory Disease.* 2012;109:11200-5.

28. Tomas-Loba A, Manieri E, Gonzalez-Teran B, Mora A, Leiva-Vega L, Santamans AM, Romero-Becerra R, Rodriguez E, Pintor-Chocano A, Feixas F, Lopez JA, Caballero B, Trakala M, Blanco O, Torres JL, Hernandez-Cosido L, Montalvo-Romeral V, Matesanz N, Roche-Molina M, A. BJ, Mischo H, Leon M, Caballero A, Miranda-Saavedra D, Ruiz-Cabello J, Nevzorova YA, Cubero FJ, Bravo J, Vazquez J, Malumbres M, Marcos M, Osuna S, and Sabio G. p38g is essential for cell cycle progression and liver tumoriogenesis. *Nature.* 2019;568:557-60.

29. Tyner JW, Kim EY, Ide K, Pelletier MR, Roswit WT, Morton JD, Battaile JT, Patel AC, Patterson GA, Castro M, Spoor MS, You Y, Brody SL, and Holtzman MJ. Blocking airway mucous cell metaplasia by inhibiting EGFR antiapoptosis and IL-13 transdifferentiation signals. *J Clin Invest.* 2006;116:309-21.

30. Patel AC, Morton JD, Kim EY, Alevy Y, Swanson S, Tucker J, Huang G, Agapov E, Phillips TE, Fuentes ME, Iglesias A, Aud D, Allard JD, Dabbagh K, Peltz G, and Holtzman MJ. Genetic segregation of airway disease traits despite redundancy of chloride channel calcium-activated (CLCA) family members. *Physiol Genomics.* 2006;25:502-13.

31. Grayson MH, Cheung D, Rohlfing MM, Kitchens R, Spiegel DE, Tucker J, Battaile JT, Alevy Y, Yan L, Agapov E, Kim EY, and Holtzman MJ. Induction of high-affinity IgE receptor on lung dendritic cells during viral infection leads to mucous cell metaplasia. *J Exp Med.* 2007;204:2759-69.

32. Agapov E, Battaile JT, Tidwell R, Hachem R, Patterson GA, Pierce RA, Atkinson JJ, and Holtzman MJ. Macrophage chitinase 1 stratifies chronic obstructive lung disease. *Am J Respir Cell Mol Biol.* 2009;41:379-84.

33. Wu K, Byers DE, Jin X, Agapov E, Alexander-Brett J, Patel AC, Cella M, Gilfilan S, Colonna M, Kober DL, Brett TJ, and Holtzman MJ. TREM-2 promotes macrophage survival and lung disease after respiratory viral infection. *J Exp Med.* 2015;212:681-97.

34. Keeler SP, Agapov EV, Hinojosa ME, Letvin AN, Wu K, and Holtzman MJ. Influenza A virus infection causes chronic lung disease linked to sites of active viral RNA remnants. *J Immunol.* 2018;201:2354-68.

35. Zhang Y, Mao D, Keeler SP, Wang X, Wu K, Gerovac BJ, Shornick LP, Agapov E, and Holtzman MJ. Respiratory enterovirus (like parainfluenza virus) can cause chronic lung disease if protection by airway epithelial STAT1 is lost. *J Immunol.* 2019;202:2332-47.

36. Wu K, Wang X, Keeler SP, Gerovac BJ, Agapov E, Byers DE, Gilfillan S, Colonna M, Zhang Y, and Holtzman MJ. Group 2 innate lymphoid cells must partner with the myeloid-macrophage lineage for long-term postviral lung disease. *J Immunol.* 2020;205:1084-101.

37. Wang X, Wu K, Keeler SP, Mao D, Agapov EV, Zhang Y, and Holtzman MJ. TLR3-activated monocyte-derived dendritic cells trigger progression from acute viral infection to chronic disease in the lung. *J Immunol.* 2021;206:1297-314 (selected for Top-Reads p. 115).

38. Keeler SP, Yantis J, Youkilis S, Podgorny S, Mao D, Zhang Y, Whitworth KM, Redel BK, Samuel MS, Wells KD, Prather RS, and Holtzman MJ. Chloride channel accessory 1 (CLCA1) gene deficiency causes selective loss of mucus production in a new pig model. *Am J Physiol Lung Cell Mol Physiol.* 2022;322:L842-L52.

39. Martin RA, Keeler SP, Wu K, Shearon WJ, Patel D, Hoang M, Hoffmann CM, Hughes ME, and Holtzman MJ. An alternative mechanism for skeletal muscle dysfunction in long-term post-viral lung disease. *bioRxiv.* 2022;10.1101/2022.10.07.511313.

40. van Nunen MCJ, and van der Veen J. Experimental infection with Sendai virus in mice. *Arch Gesamte Virusforsch.* 1967;22:388-97.

41. Livak KJ, and Schmittgen TD. Analysis of relative gene expression data using real-time quantitative PCR and the 2(-Delta Delta C(T)) Method. *Methods.* 2001;25:402-8.

42. Wu K, Zhang Y, Yin-Declue H, Sun K, Mao D, Austin S, Crouch E, Brody S, Byers D, Hoffmann C, Hughes M, and Holtzman M. A correctable immune niche for basal-epithelial stem cell reprogramming and post-viral lung diseases. *J Clin Invest.* 2024;134:e183092.

43. Deslee G, Woods J, Moore C, Conradi S, Gierada D, Atkinson J, Battaile J, Liu L, Patterson A, Adair-Kirk T, Holtzman M, and Pierce R. Oxidative damage to nucleic acids in severe emphysema. *Chest.* 2009;135:965-74.

44. Byers DE, Wu K, Dang-Vu G, Jin X, Agapov E, Zhang X, Battaile JT, Schechtman KB, Yusen R, Pierce RA, and Holtzman MJ. Triggering receptor expressed on myeloid cells-2 (TREM-2) expression tracks with M2-like macrophage activity and disease severity in COPD. *Chest.* 2018;153:77-86.

45. Keeler SP, Wu K, Zhang Y, Mao D, Li M, Iberg CA, Austin SP, Glaser SA, Yantis J, Podgorny S, Brody SL, Chartock JR, Han Z, Byers DE, Romero AG, and Holtzman MJ. A potent MAPK13-14 inhibitor prevents airway inflammation and mucus production. *Am J Physiol Lung Cell Mol Physiol.* 2023;325:L726-40.

46. Holtzman M, Zhang Y, Wu K, and Romero AG. Mitogen-activated protein kinase-guided drug discovery for post-viral and related types of lung disease. *Eur Respir Rev.* 2024;33:230220.

47. Holtzman MJ, Zhang Y, Wu K, and Romero AG. Mitogen-activated protein kinase-guided drug discovery for post-viral and related types of lung disease. *Eur Respir Rev.* 2024;33:230220.

48. Sabio G, Simon J, Arthur C, Kuma Y, Peggie M, Carr J, Murray-Tait V, Centeno F, Goedert M, Morrice NA, and Cuenda A. p38g regulates the localisation of SAP97 in the cytoskeleton by modulating its interaction with GKAP. *EMBO J.* 2005;24:1134-45.

49. Zur R, Garcia-Ibanez L, Nunez-Buiza A, Aparicio N, Liappas G, Escos A, Risco A, Page A, Saiz-Ladera C, Alsina-Beauchamp D, Montans J, Paramio JM, and Cuenda A. Combined deletion of p38gamma and p38delta reduces skin inflammation and protects from carcinogenesis. *Oncotarget.* 2015;6(15):12920-35.

50. Gonzalez-Teran B, Lopez JA, Rodriguez E, Leiva L, Martinez-Martinez S, Bernal JA, Jimenez-Borreguero LJ, Redondo JM, Vazquez J, and Sabio G. p38gamma and delta promote heart hypertrophy by targeting the mTOR-inhibitory protein DEPTOR for degradation. *Nat Commun.* 2016;7:10477.

51. Alsina-Beauchamp D, Escos A, Fajardo P, Gonzalez-Romero D, Diaz-Mora E, A. R, Martin-Serrano MA, C. dF, Dominguez-Andres J, Aparicio N, Zur R, Shpiro N, Brown GD, Ardavin C, Netea MC, Alemany S, Sanz-Ezquerro JJ, and Cuenda A. Myeloid cell deficiency of p38g/p38d protects against candidiasis and regulates antifungal immunity. *EMBO Mol Med.* 2018;10:e8485.

52. Barrio L, Roman-Garcia S, Diaz-Mora E, Risco A, Jimenez-Saiz R, Carrasco YR, and Cuenda A. B Cell Development and T-Dependent Antibody Response Are Regulated by p38gamma and p38delta. *Front Cell Dev Biol.* 2020;8:189.

53. Escos A, Martin-Gomez J, Gonzalez-Romero D, Diaz-Mora E, Francisco-Velilla R, Santiago C, Cueza J, Dominguez-Zorita S, Martinez-Salas E, Sonenberg N, Sanz-Ezquerro J, Jafanejad S, and Cuenda A. TPL2 kinase expression is regulated by the p38g/p38d-dependent association with aconitase-1 with *TPL2* mRNA. *Proc Natl Acad Sci U S A.* 2022;119:e2204752119.

54. Escos A, Diaz-Mora E, Pattison M, Fajardo P, Gonzalez-Romero D, Risco A, Martin-Gomez J, Bonnell E, Sonenberg N, Jafanejad SM, Sanz-Ezquerro JJ, Ley SC, and Cuenda A. p38g and p38d modulate innate immune response by regulating MEF2D activation. *eLife.* 2023;12:e86200.

55. Underwood DC, Osborn RR, and Kotzer CJ. SB 239063, a potent p38 MAP kinase inhibitor, reduces inflammatory cytokine production, airways eosinophil infiltration, and persistence. *J Pharmacol Exp Ther.* 2000;293:281-8.

56. Duan W, Chan JH, McKay K, Crosby JR, Choo HH, Leung BP, Karras JG, and Wong WSF. Inhaled p38alpha mitogen-activated protein kinase antisense oligonucleotide attenuates asthma in mice. *Am J Respir Crit Care Med.* 2005;171:571-8.

57. Medicherla S, Fitzgerald MF, Spicer D, Woodman P, Ma JY, Kapoun AM, Chakravarthy S, Dugar S, Protter AA, and Higgins LS. p38a-selective mitogen-activated protein kinase inhibitor SD-282 reduces inflammation in a subchronic model of tobacco smoke-induced airway inflammation. *J Pharmacol Exp Ther.* 2008;324:921-9.

58. Renda T, Baraldo S, Pelaia G, Bazzan E, Turato G, Papi A, Maestrelli P, Maselli R, Vatrella A, Fabbri LM, Zuin R, Marsico SA, and Saetta M. Increased activation of p38 MAPK in COPD. *Eur Respir J.* 2008;31:62-9.

59. MacNee W, Allan RJ, Jones I, Cristina De Salvo M, and Tan LF. Efficacy and safety of the oral p38 inhibitor PH-797804 in chronic obstructive pulmonary disease: a randomised clinical trial. *Thorax.* 2013;68:738-45.

60. Kawai T, and Akira S. Pathogen recognition with Toll-like receptors. *Curr Opin Immunol.* 2005;17(4):338-44.

61. Ha U, H. LJ, Jono H, Koga T, Srivastava A, Malley R, Pages G, Pouyssegur J, and Li J-D. A novel role for IkB kinase (IKK) a and IKKb in ERK-dependent up-regulation of MUC5AC mucin transcription by Streptococcus pneumoniae. *J Immunol.* 2007;178:1736-47.

62. Fujisawa T, Velichko S, Thai P, Hung LY, Huang F, and Wu R. Regulation of airway MUC5AC expression by IL-1beta and IL-17A; the NF-kappaB paradigm. *J Immunol.* 2009;183(10):6236-43.

63. Na HG, Kim Y-D, and Bae CH. High concentration of insulin induces MUC5AC expression via phosphoinositide 3 kinase/AKT and mitogen-activated protein kinase signaling pathways in human airway epithelial cells. *Am J Rhinol Allergy.* 2018.

64. Xu H, Sun Q, Lu L, Luo F, Zhou L, Liu J, Cao L, Wang Q, Xue J, Yang Q, Yang P, Lu J, Xiang Q, and Liu Q. MicroRNA-218 acts by repressing TNFR1-mediated activation of NF-kB, which is involved in MUC5AC hyper-production and inflammation in smoking-induced bronchiolitis of COPD. *Toxicol Lett.* 2017;280:171-80.

65. Wu S, Li H, Yu L, Wang N, Li X, and Chen W. IL-1b upregulates Muc5ac expression via NF-kB-induced HIF-1a in asthma. *Immunol Lett.* 2017;192:20-6.

66. Selness SR, Devraj RV, Devadas B, Walker JK, Boehm TL, Durley RC, Shieh H, Xing L, Rucker PV, Jerome KD, and Benson AG. Discovery of PH-797804, a highly selective and potent inhibitor of p38 MAP kinase. *Bioorg Med Chem Lett.* 2011;21:4066-71.

67. McQualter JL, Yuen K, Williams B, and Bertoncello I. Evidence of an epithelial stem/progenitor cell hierarchy in the adult mouse lung. *Proc Natl Acad Sci U S A.* 2010;107(4):1414-9.

68. Tarutani M, Itami S, Okabe M, Ikawa M, Tezuka T, Yoshikawa K, Kinoshita T, and Takeda J. Tissue-specific knockout of the mouse Pig-a gene reveals important roles for GPI-anchored proteins in skin development. *American Review of Respiratory Disease.* 1997;94:7400-5.

69. Varjosalo M, Keskitalo S, Van Drogen A, Nurkkala H, Vichalkovski A, Aebersold R, and Gstaiger M. The protein interaction landscape of the human CMGC kinase group. *Cell Rep.* 2013;3(1306-1320).

70. Sigurs N, Aljassim F, Kjellman B, Robinson PD, Sigurbergsson F, Bjarnason R, and Gustafsson PM. Asthma and allergy patterns over 18 years after severe RSV bronchiolitis in the first year of life. *Thorax.* 2010;65(12):1045-52.

71. Holtzman MJ, Byers DE, Alexander-Brett J, and Wang X. The role of airway epithelial cells and innate immune cells in chronic respiratory disease. *Nat Rev Immunol.* 2014;14:686-98.

72. Mallia P, Message SD, Gielen V, Contoli M, Gray K, Kebadze T, Aniscenko J, Laza-Stanca V, Edwards MR, Slater L, Papi A, Stanciu LA, Kon OM, Johnson M, and Johnston SL. Experimental rhinovirus infection as a human model of chronic obstructive pulmonary disease exacerbation. *Am J Respir Crit Care Med.* 2011;183:734-42.

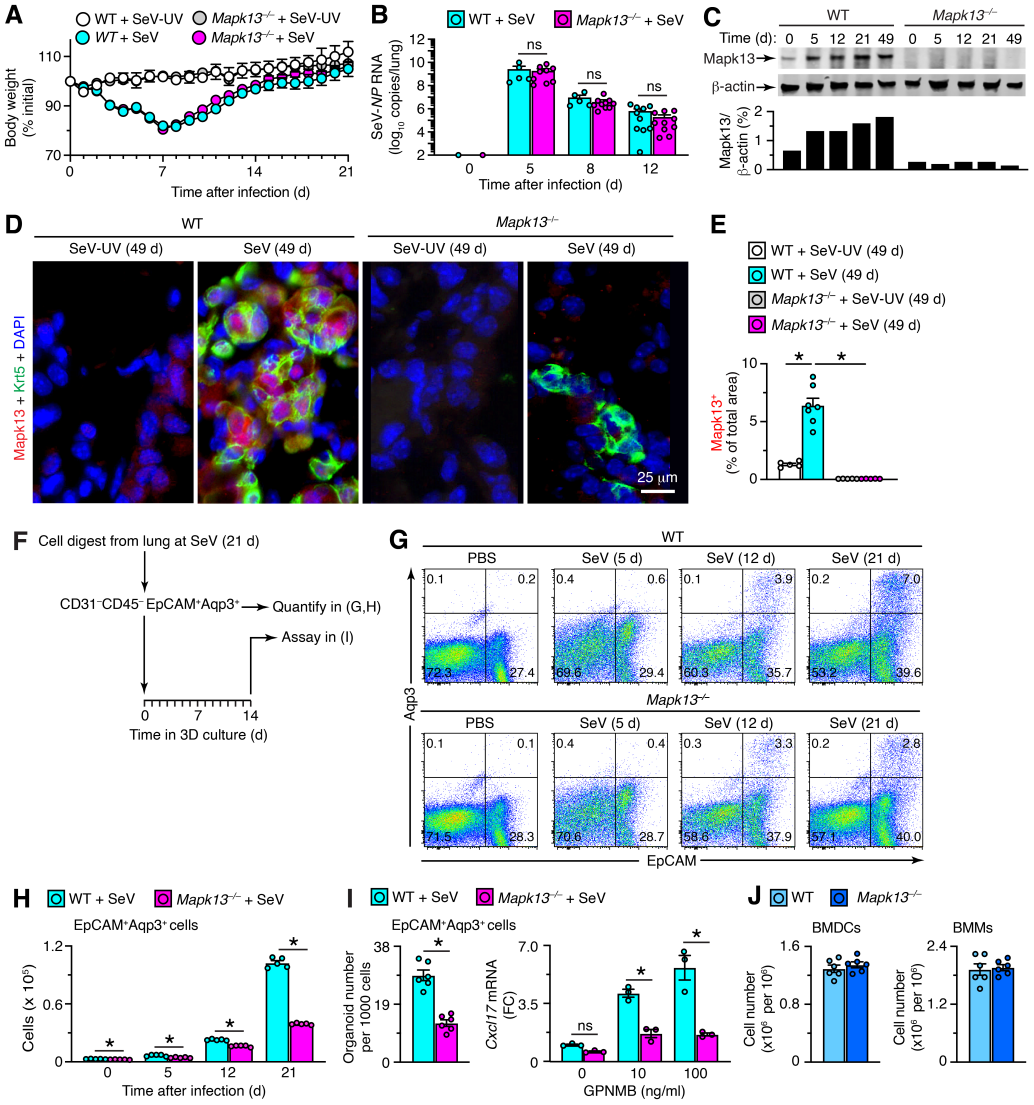

Fig. 1. *Mapk13* gene-knockout attenuates basal-ESC hyperplasia/metaplasia in a mouse model of post-viral lung disease (PVLD). A, Body weights for wild-type (WT) and *Mapk13*$^{-/-}$ mice after infection with Sendai virus (SeV) or SeV-UV control. **B,** SeV-*PA* RNA levels in lung tissue from WT and *Mapk13*$^{-/-}$ mice after SeV or SeV-UV. **C,** Levels of Mapk13 in lung tissue obtained from WT and *Mapk13*$^{-/-}$ mice after SeV infection. **D**, Immunostaining for Mapk13 and Krt5 with DAPI counterstaining in lung sections from WT and *Mapk13*$^{-/-}$ mice at 49 d after SeV or SeV-UV. **E**, Quantitation of Mapk13 immunostaining for (C). **F**, Protocol for mouse basal epithelial cell (mBEC) study using EpCAM^{+}Aqp3^{+} lung epithelial cells isolated from mice at 21 d after SeV infection. **G,** Flow cytograms of lung epithelial cells (CD31^{-}CD45^{-}EpCAM^{+}Aqp3^{+}) after SeV or SeV-UV. Values indicate the percentage of cells within each gate. **H**, Cell numbers for conditions in (G). **I,** Levels of organoid growth and *Cxcl17* mRNA in mBEC cultures from WT or *Mapk13*$^{-/-}$ mice for conditions in (F). **J**, Levels of growth for bone-marrow derived dendritic cells (BMDCs) and monocytes (BMMs) from WT and *Mapk13*$^{-/-}$ mice. Values represent mean ± s.e.m. (n=6-8 mice per condition). *P <0.05 by ANOVA and Tukey correction; ns, not statistically significant.

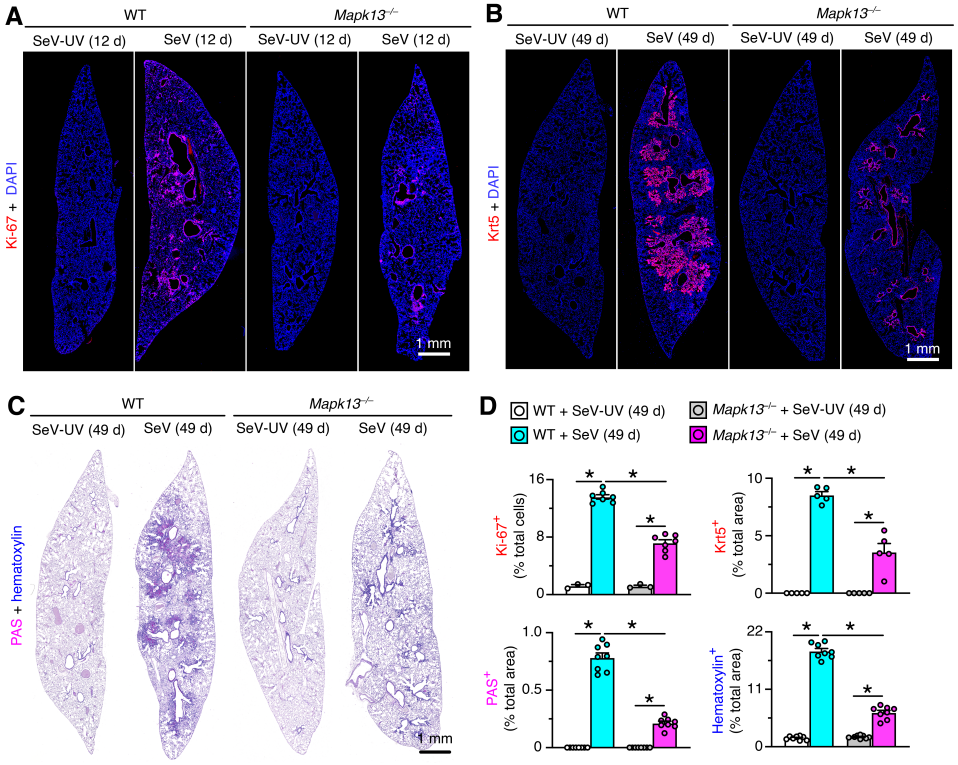

Fig. 2. *Mapk13* gene-knockout attenuates basal-ESC hyperplasia/metaplasia and histopathology in a mouse model of PVLD. A, Immunostaining for Ki-67 and counterstaining for DAPI in lung sections from mice at 12 d after SeV or SeV-UV. **B,** Immunostaining for Krt5 with DAPI counterstaining in lung sections from mice at 49 d after SeV or SeV-UV. **C**, PAS and hematoxylin staining of lung sections for conditions in (B). **D**, Quantitation of staining for (A-C). Values represent mean ± s.e.m. (n=5-8 mice per condition). Values represent mean ± s.e.m. *P <0.05 by ANOVA.

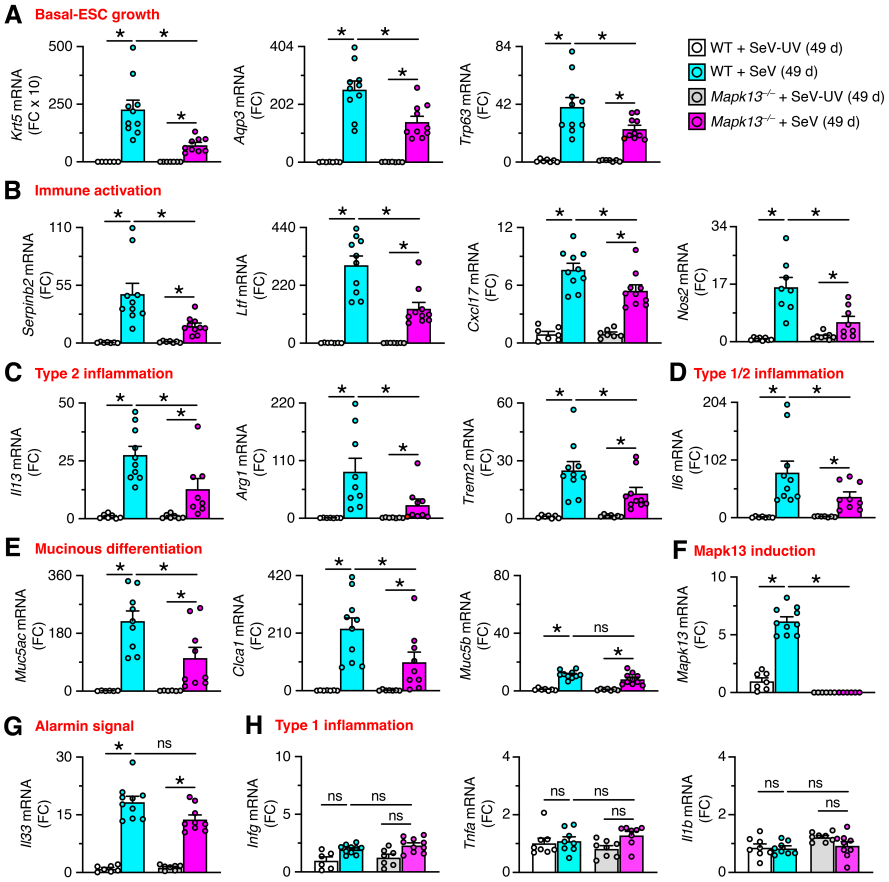

Fig. 3. *Mapk13* gene-knockout attenuates mRNA biomarkers of PVLD. A-H, Lung tissue levels of mRNA biomarkers in WT and *Mapk13*$^{-/-}$ mice at 49 d after SeV or SeV-UV to track basal-ESC growth (A), immune activation (B), type 2 inflammation (C), type 1/2 inflammation (D), mucinous differentiation (E), Mapk13 induction (F), alarmin signal (G), and type 1 inflammation (H). Values represent mean ± s.e.m. (n=10 mice per condition). *P <0.05 by ANOVA and Tukey correction; ns, not statistically significant.

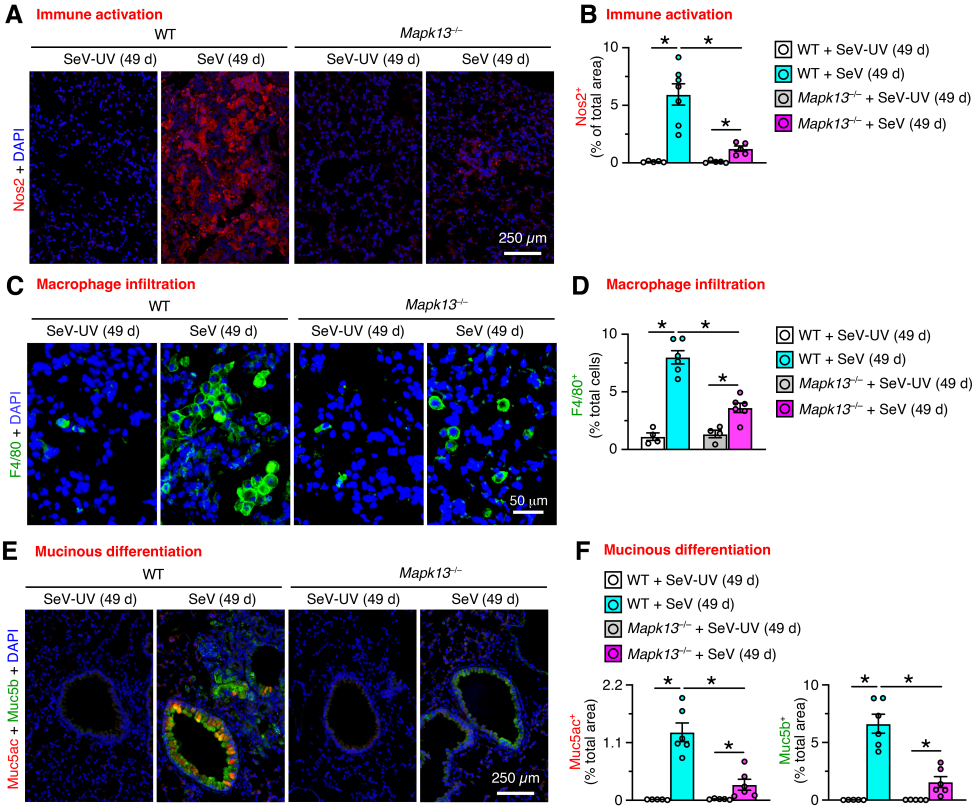

Fig. 4. *Mapk13* gene-knockout attenuates clinical phenotypes of PVLD. A, Immunostaining of lung sections for Nos2 with DAPI counterstaining of lung sections from WT and *Mapk13*$^{-/-}$ mice at 49 d after SeV or SeV-UV. **B**, Quantitation of immunostaining for (A). **C.** Immunostaining for F4/80 with DAPI counterstaining of lung sections for conditions (A). **D**, Quantitation of staining for (C). **E,** Immunostaining of lung sections for Muc5ac and Muc5b with DAPI counterstaining for conditions in (A). **F,** Quantitation of staining for (e). Values represent mean ± s.e.m. (n=5-9 mice per condition). *P <0.05 by ANOVA and Tukey correction.

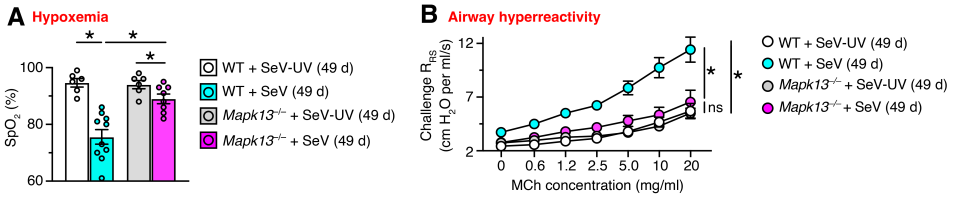

Fig. 5. *Mapk13* gene-knockout attenuates functional readouts of PVLD. A, Oximeter levels for blood oxygen saturation (SpO_2) for WT and *Mapk13*$^{-/-}$ mice at 49 d after SeV or SeV-UV. **B,** Values for respiratory system resistance (R_{RS}) at baseline and after inhaled methacholine (MCh) for conditions in (A). Values represent mean ± s.e.m. (n=5-9 mice per condition). *P <0.05 by ANOVA and Tukey correction.

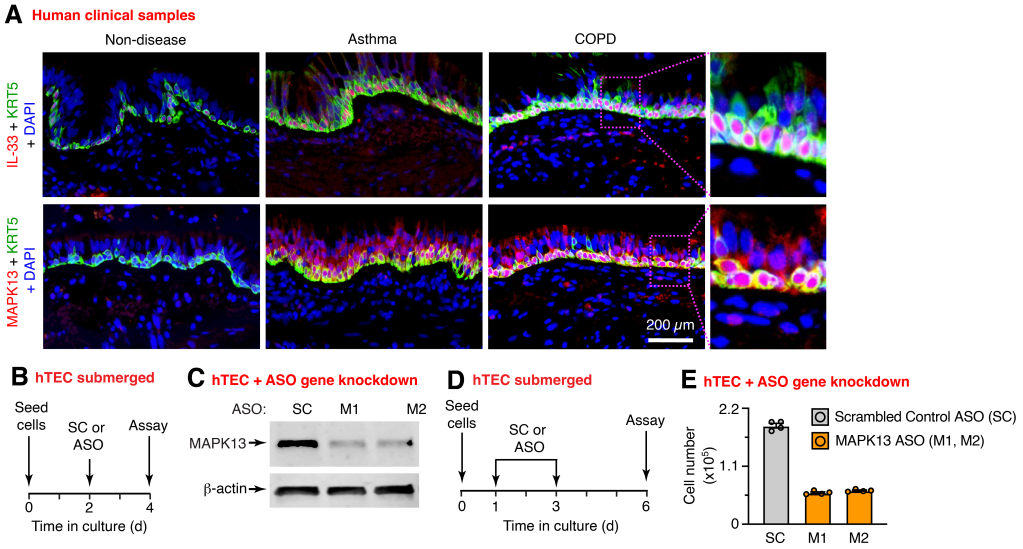

Fig. 6. MAPK13 is activated in chronic lung disease and is required for basal-ESC growth. **A**, Representative immunostaining for IL-33 plus KRT5 or MAPK13 plus KRT5 with DAPI counterstaining in lung sections from non-disease control (n=11), asthma (n=10), and COPD (n=10) subjects (inset, 5x). **B,** Protocol for human tracheobronchial epithelial cell (hTEC) study using 2D culture under submerged conditions and *MAPK13* mRNA knockdown with anti-sense oligonucleotide (ASO) or scrambled control (SC). **C,** Western blot for conditions in (B). D, Protocol modified from (B) for *MAPK13* mRNA knockdown effect on cell number. **E**, Cell numbers for conditions in (D). Values represent mean ± s.e.m. for a single subject representative of 3 subjects.

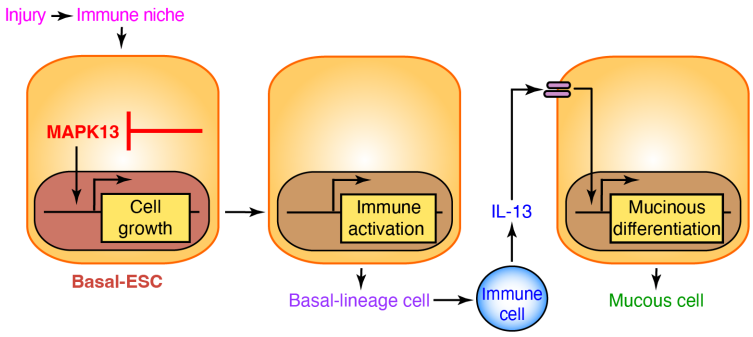

Fig. 7. Scheme for MAPK13 control of structural remodeling and disease after lung injury. Sequential steps include: lung epithelial injury (e.g., viral injury) and then basal-ESC growth and immune activation, immune cell production of inflammatory cytokines (e.g., IL-13), and in turn basal-ESC mucinous differentiation to mucous cells.